PNAS RESEARCH ARTICLE | MICROBIOLOGY

DsrMKJOP is the terminal reductase complex in anaerobic sulfate respiration

Ana C. C. Barbosa[a,1], Sofia S. Venceslau[a,1,2], and Inês A. C. Pereira[a,2]

Edited by Bo Barker Jorgensen, Aarhus University, Brabrand, Denmark; received August 8, 2023; accepted December 20, 2023

Microbial dissimilatory sulfate reduction (DSR) is a key process in the Earth biogeochemical sulfur cycle. In spite of its importance to the sulfur and carbon cycles, industrial processes, and human health, it is still not clear how reduction of sulfate to sulfide is coupled to energy conservation. A central step in the pathway is the reduction of sulfite by the DsrAB dissimilatory sulfite reductase, which leads to the production of a DsrC-trisulfide. A membrane-bound complex, DsrMKJOP, is present in most organisms that have DsrAB and DsrC, and its involvement in energy conservation has been inferred from sequence analysis, but its precise function was so far not determined. Here, we present studies revealing that the DsrMKJOP complex of the sulfate reducer *Archaeoglobus fulgidus* works as a menadiol:DsrC-trisulfide oxidoreductase. Our results reveal a close interaction between the DsrC-trisulfide and the DsrMKJOP complex and show that electrons from the quinone pool reduce consecutively the DsrM hemes *b*, the DsrK noncubane [4Fe-4S]$^{3+/2+}$ catalytic center, and finally the DsrC-trisulfide with concomitant release of sulfide. These results clarify the role of this widespread respiratory membrane complex and support the suggestion that DsrMKJOP contributes to energy conservation upon reduction of the DsrC-trisulfide in the last step of DSR.

sulfur metabolism | sulfate-reducing bacteria | dissimilatory sulfite reductase | dissimilatory sulfate reduction

Significance

Dissimilatory sulfate reduction (DSR) is a vital microbial process in anoxic marine, freshwater, and terrestrial environments. DSR drives the global biogeochemical sulfur cycle and plays key roles in remineralization of organic matter, in well-recognized or cryptic sulfur cycling, and prevention of methane production from both freshwater and marine sediments. It has also health implications related to excessive sulfide production in the mammalian gut. Despite its high ecological importance, it is still not clear how microorganisms derive energy to grow through DSR. Here, we disclose the physiological function of a widespread membrane complex in DSR, showing it acts as the terminal reductase in the respiratory chain and providing important insights into how sulfate/sulfite reduction is linked to energy conservation.

Sulfur is a key element for life, mainly due to its chemical versatility and ability to switch between several biologically relevant oxidation states, ranging from -II, as in hydrogen sulfide (H_2S), up to +VI, as in sulfate (SO_4^{2-}). A critically important microbial process in the biogeochemical sulfur cycle is dissimilatory sulfate reduction (DSR) driven by anaerobic bacteria and archaea, in which the reduction of sulfate to hydrogen sulfide is linked to energy conservation (1, 2). This process has particular impact in marine sediments and oxygen minimum zones, accounting for up to 50% of carbon mineralization in the sea floor (3), and preventing methane emissions through its contribution to anaerobic methane oxidation (4, 5). Sulfate/sulfite reduction also plays an important role in cryptic sulfur cycling in various freshwater and deep marine environments (6), as well as in the mammalian gut (7), where it has been implicated in inflammatory bowel diseases (8) and colorectal cancer (9). Despite being a very ancient bioenergetic pathway (10), it is still not fully clear how sulfate reducers conserve energy during sulfate respiration, although an electrogenic complex present in many organisms has been identified (11), and models have been proposed (12–14). In DSR, a central step is the reduction of sulfite, performed by the dissimilatory sulfite reductase DsrAB and its physiological partner DsrC, which mediate a four-electron reduction of sulfite to zero-valent sulfur in the form of a trisulfide formed between two conserved cysteines of DsrC (12, 14, 15). The reduction of the DsrC-trisulfide to hydrogen sulfide is thought to derive electrons from the quinone pool via the membrane-bound DsrMKJOP complex, pointing to a critical role of this complex in energy conservation (14, 16, 17). The Dsr proteins, namely DsrAB, DsrC, and DsrMKJOP, are widespread in the microbial world, being also present in phototrophic and chemotrophic sulfur-oxidizing organisms where they are involved in sulfite oxidation (18, 19), and in many organisms capable of sulfur, thiosulfate, sulfite, or organosulfonates reduction and in sulfur disproportionators (6, 20, 21). However, there is still no concrete evidence demonstrating the physiological function of the DsrMKJOP complex.

The DsrMKJOP complex was first isolated and characterized from *Archaeoglobus fulgidus* (22), then from *Desulfovibrio desulfuricans* (17), and later from *Allochromatium vinosum* (23), where this complex has been shown to be essential for sulfur globule oxidation (24). This transmembrane complex contains two periplasmic subunits (DsrJ and DsrO), two integral membrane subunits (DsrM and DsrP) and a cytoplasmic subunit (DsrK), and appears to be composed of a combination of two modules, DsrMK and DsrJOP (25). The MK module is homologous to the membrane-bound heterodisulfide reductase (Hdr) HdrED from methanogens (26–28), comprising a quinone-interacting membrane diheme

Author affiliations: [a]Instituto de Tecnologia Química e Biológica António Xavier, Universidade Nova de Lisboa, Oeiras 2780-156, Portugal

Author contributions: S.S.V. and I.A.C.P. designed research; A.C.C.B. and S.S.V. performed research; A.C.C.B., S.S.V., and I.A.C.P. analyzed data; and A.C.C.B., S.S.V., and I.A.C.P. wrote the paper.

The authors declare no competing interest.

This article is a PNAS Direct Submission.

[1]A.C.C.B. and S.S.V. contributed equally to this work.

[2]To whom correspondence may be addressed. Email: sofiasvenceslau@gmail.com or ipereira@itqb.unl.pt.

This article contains supporting information online at https://www.pnas.org/lookup/suppl/doi:10.1073/pnas.2313650121/-/DCSupplemental.

Published January 29, 2024.

cytochrome *b* DsrM, with both hemes displaying His/His coordination, and an iron–sulfur subunit DsrK predicted to have two canonical $[4Fe\text{-}4S]^{2+/1+}$ clusters, and one noncubane $[4Fe\text{-}4S]^{3+/2+}$ cluster (17). The noncubane cluster is predicted on the basis of a conserved five-cysteine motif $CX_nCCGX_nCX_2C$ (the CCG motif) (29), which was identified to bind the catalytic noncubane cluster for heterodisulfide reduction in the homologous HdrD (22). The DsrJOP module contains DsrP, an integral membrane subunit with ten predicted transmembrane helices, and DsrO, an iron–sulfur subunit predicted to coordinate three to four $[4Fe\text{-}4S]^{2+/1+}$ clusters, which together resemble the quinone-interacting NrfCD module widespread in bacterial oxidoreductases (30). DsrJ is a membrane-anchored triheme cytochrome *c*, where each heme is proposed to have distinct axial coordination: His/His, His/Met, and His/Cys (17, 31). The His/Cys heme *c* coordination is very unusual but is also found in SoxXA (32), TdsA (33), and PufC (34), which are involved in thiosulfate oxidation and/or electron transfer, suggesting that DsrJ could have a catalytic role in sulfur redox chemistry. Notably, the DsrJOP module is absent in many gram-positive Bacillota (formerly known as Firmicutes) and archaeal sulfate reducers (6, 25) and so does not seem to be essential. In contrast, the DsrMK proteins are present in all organisms containing DsrAB and DsrC, often encoded in the same operon and sometimes with multiple copies in the genome, which suggests that this is the minimum functional module of this respiratory complex (25). Based on its similarity to HdrED, the DsrMK module was proposed to catalyze the reduction of DsrC-trisulfide to hydrogen sulfide through the oxidation of the quinone pool (14, 16, 17, 35). However, the presence of the DsrJOP module suggests that there may be a more elaborate mechanism (14). Both DsrM and DsrP are homologous to quinone-interacting proteins, and the presence of two putative quinone-binding sites led to the suggestion that a quinone cycle between the DsrMK and DsrJOP modules may be present (16).

The X-ray structure of the soluble HdrABC-MvhAGD complex from the methanogenic archaeon *Methanothermococcus thermolithotrophicus*, comprising the MvhAGD hydrogenase and the HdrABC Hdr, provided structural insights into the two noncubane $[4Fe\text{-}4S]^{3+/2+}$ clusters present in the active site of HdrB, and how they mediate the reduction of CoM-S-S-CoB heterodisulfide (36). Each noncubane cluster is ligated by five cysteines from the predicted CCG motif. There are two such motifs in both HdrB and HdrD, the catalytic subunits of the two different types of Hdrs in methanogens. Cleavage of the CoM-S-S-CoB disulfide bond has been suggested to involve the two noncubane clusters in a homolytic mechanism, along with binding of each substrate to one of the clusters (36). Remarkably, only one CCG motif is present in DsrK, raising the question of how this protein may operate with a single noncubane cluster. Recently, studies of the noncubane $[4Fe\text{-}4S]^{3+/2+}$ cluster in the HdrB protein from *Desulfovibrio vulgaris* Hildenborough revealed that this cluster can adopt "closed" and "open" conformations corresponding to the substrate-free and substrate-bound forms, respectively (37), suggesting that cluster flexibility may be important for binding the DsrC-trisulfide in the active site of its homolog, DsrK.

Overall, unraveling the role of the DsrMKJOP complex and its link to DsrC-trisulfide reduction and corresponding energy conservation mechanism is a major challenge in understanding dissimilatory sulfur metabolism. In the present study, we provide evidence for the activity of the DsrMKJOP complex as a menadiol:DsrC-trisulfide oxidoreductase, clarifying the functional role of this membrane complex in the final step of the sulfate respiratory chain, where it is likely coupled to energy conservation.

Results and Discussion

DsrMKJOP Isolation and Reduction with Menadiol. The DsrMKJOP transmembrane complex was purified with DDM as solubilizing detergent from membranes of the thermophilic archaeon *A. fulgidus,* by adapting the protocol previously reported by Mander et al. (22). The DsrMKJOP complex is the only heme-containing membrane complex in *A. fulgidus* (25), which facilitates its purification compared with other sulfate reducers, such as *D. desulfuricans* (17). In *A. fulgidus*, the predicted molecular mass for each subunit of the complex is 38.4 kDa (DsrM, locus tag: AF0501), 64.4 kDa (DsrK, AF0502), 16.7 kDa (DsrJ, AF0503), 30.5 kDa (DsrO, AF0499), and 44.2 kDa (DsrP, AF0500). The purified complex displayed four bands on a Tricine-sodium dodecyl-sulfate polyacrylamide gel electrophoresis (SDS-PAGE) gel (*SI Appendix*, Fig. S1) with apparent molecular masses of 61, 31, 28, and 17 kDa, in line with the report by Mander et al. (22). The 17-kDa band was identified as a cytochrome *c* (DsrJ) by heme-staining, and the other bands were assigned as DsrK (61 kDa), DsrM (31 kDa), and DsrO (28 kDa), based on previous identifications (17, 22). As reported before, DsrP is not detected by SDS-PAGE (17, 22) because it is a highly hydrophobic subunit (ten predicted transmembrane helices), which hinders its migration in the gel.

The UV–visible spectrum of the as-purified DsrMKJOP (oxidized state) is dominated by absorption maxima at 280, 410, and 527 nm (Fig. 1*A*), confirming the presence of hemes. Upon reduction, the Soret peak shifts to 421 nm, and the β- and α-bands are

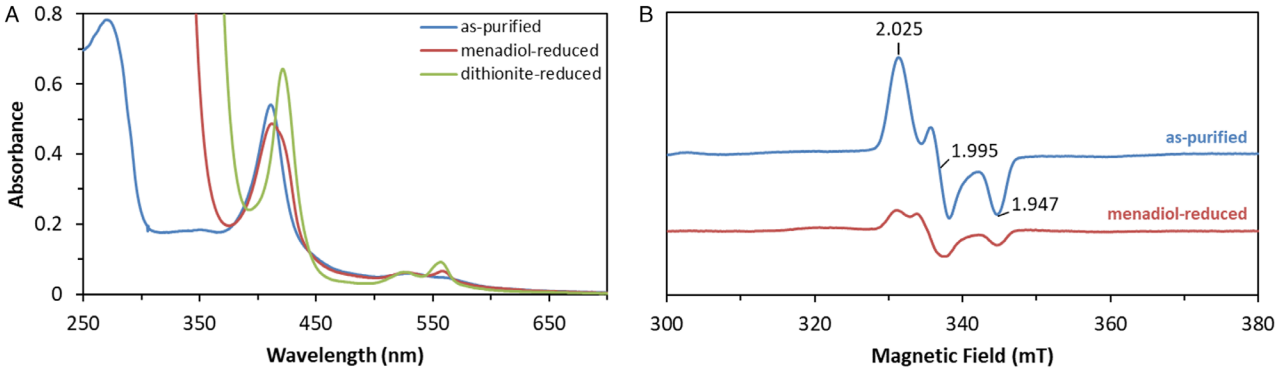

Fig. 1. UV–visible and EPR spectroscopy of the *A. fulgidus* DsrMKJOP complex. (*A*) UV–visible spectra of as-purified DsrMKJOP (0.7 μM) (blue), menadiol-reduced (red), and dithionite-reduced (green). (*B*) EPR spectra of the $[4Fe\text{-}4S]^{3+/2+}$ cluster of the as-purified DsrMKJOP (blue), and upon menadiol reduction (red). *g*-values are marked in the spectrum of as-purified DsrMKJOP. The menadiol reduction spectra (UV-Vis and EPR) were obtained in a 1:500 protein to menadiol ratio.

observed at 524 and 557 nm, respectively, which is in line with previously reported spectra of DsrMKJOP from *A. fulgidus* (22) and *D. desulfuricans* (17). The α-band is quite broad supporting the presence of hemes *b* and *c*. Addition of menadiol reduced 38% of the total hemes as compared with full reduction by dithionite. This corresponds to approximately two hemes reduced, and since hemes *b* typically have higher redox potentials than hemes *c,* this likely corresponds to the two predicted hemes *b* in the quinone-interacting DsrM membrane subunit. A similar result was reported by Pires et al. (17), where 40% of hemes belonging to the *D. desulfuricans* DsrMKJOP were also reduced upon incubation with menadiol.

The electron paramagnetic resonance (EPR) spectrum of the as-purified *A. fulgidus* DsrMKJOP shows an intense rhombic signal characteristic of a noncubane $[4Fe\text{-}4S]^{3+/2+}$ cluster in the oxidized state, with *g*-values of 2.025, 1.995, and 1.947 (Fig. 1*B*). This EPR signature was first observed in Hdrs from methanogens (upon addition of HS-CoM or HS-CoB), with *g*-values of 2.013, 1.991, and 1.938 for HdrABC from *Methanothermobacter marburgensis* and 2.012, 1.993, and 1.946 for HdrED from *Methanosarcina barkeri* (38, 39), both of which possess two noncubane $[4Fe\text{-}4S]^{3+/2+}$ catalytic centers involved in mediating heterodisulfide (CoM-S-S-CoB) reduction in two one-electron steps (28, 40). The previously reported *g*-values of *A. fulgidus* DsrMKJOP were 2.031, 1.994, and 1.941 (22), while in *D. desulfuricans* DsrMKJOP the *g*-values were 2.027, 1.991, and 1.943 (17). Given the similarity of DsrK to HdrD, the noncubane $[4Fe\text{-}4S]^{3+/2+}$ cluster present in DsrK is likely involved in thiol/disulfide chemistry, with DsrK being the catalytic subunit of the DsrMKJOP complex, as previously suggested (14). Upon incubation with menadiol under anoxic conditions, the intensity of the rhombic signal decreased by 85% (Fig. 1*B*), revealing a pathway for electron transfer from the hemes *b* of DsrM to the noncubane $[4Fe\text{-}4S]^{3+/2+}$ cluster of DsrK. The redox potential of the noncubane center in *A. fulgidus* DsrK was previously determined to be +90 mV (22), which agrees with its reduction by menadiol (midpoint potential of approx. −70 mV).

The DsrC-Trisulfide Interacts Strongly with DsrMKJOP. In *A. vinosum*, coelution upon protein purification suggested that DsrK interacts with DsrC (23). Following our identification of the DsrC-trisulfide as the product of sulfite reduction by DsrAB, we proposed that this is the actual substrate for the DsrMKJOP complex (14). To assess whether there is a protein–protein interaction between the DsrC-trisulfide and the DsrMKJOP complex, surface plasmon resonance (SPR) was initially used. SPR is a highly sensitive technique for studying protein–protein interactions, without the need for labeling. The *A. fulgidus* DsrC-trisulfide was produced by in vitro enzymatic reaction using DsrAB from the same organism, as described in Santos et al. (14). The DsrC-trisulfide thus produced was immobilized on a nitrilotriacetic acid (NTA) sensor chip by the N-terminal His-tag, and the interaction was studied with increasing concentrations of DsrMKJOP complex (Fig. 2). A strong interaction was observed between the two proteins, as revealed by the presence of a signal for the association and dissociation at low concentrations of the membrane complex. Steady-state conditions could not be achieved (even by increasing the association time), which means that no kinetic model could fit the experimental data, and so the association and dissociation rate constants could not be obtained. Nevertheless, an estimate for the equilibrium dissociation constant (K_D) of 200 ± 27 nM was derived from duplicate sensorgrams using the maximum response reached. This K_D confirms a strong interaction between the DsrC-trisulfide and the DsrMKJOP complex [strong interactions are in

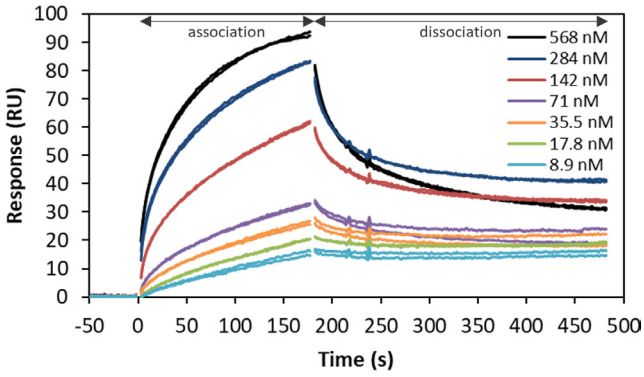

Fig. 2. Interaction assays between DsrC-trisulfide and DsrMKJOP complex. SPR sensorgrams of DsrC-trisulfide interaction with increasing concentrations of DsrMKJOP (8.9 to 568 nM), revealing the association (up to 180 s) and dissociation (>180 s) phases. Sensorgrams were measured in duplicate.

the nanomolar range, or even lower as in the case of high-affinity antibodies (41)], supporting the DsrC-trisulfide as a possible substrate for the membrane-bound DsrMKJOP complex. The SPR data were obtained at 25 °C, whereas a higher temperature (as used in the activity assays) should increase the association and dissociation rates of DsrC-trisulfide to DsrMKJOP complex since *A. fulgidus* is a thermophile, suggesting that the actual K_D at physiological temperatures may be somewhat different, and possibly even lower.

The DsrC-Trisulfide Is Reduced by DsrMKJOP. Given that menadiol can reduce the noncubane $[4Fe\text{-}4S]^{3+/2+}$ catalytic center of DsrK, and that the DsrC-trisulfide interacts with the DsrMKJOP complex, we tested whether the DsrC-trisulfide can serve as substrate and electron acceptor for the menadiol-reduced DsrMKJOP complex. Menadiol:DsrC-trisulfide oxidoreductase activity by the DsrMKJOP complex was thus measured. These experiments confirmed a fast oxidation of menadiol (measured by menadione formation at 270 nm) in the presence of the DsrC-trisulfide with a specific activity of 85.5 ± 5.4 mU/mg, assuming DsrMKJOP as a 5-subunit monomer (200 kDa) (Fig. 3*A*). In control reactions without DsrMKJOP, menadiol, or DsrC-trisulfide, no activity was detected. In addition, sequential additions of DsrC-trisulfide, after the reaction has stopped, trigger a new phase of menadiol oxidation confirming it had stopped due to substrate depletion (Fig. 3*B*).

The redox state of DsrC, before and after the reaction, was analyzed by a gel-shift assay using MalPEG, which selectively labels cysteine thiol groups (14, 42). In this assay, the DsrC-trisulfide presents no shift in the gel as it cannot bind MalPEG, whereas the reduced form binds one or two MalPEG molecules, as the last Cys_A is more accessible for labeling than Cys_B (Cys^{114} and Cys^{103} in *A. fulgidus*, respectively) (14, 42). At time zero (T_0), most DsrC shows no shift, as expected for the trisulfide, but a small amount of reduced species is present, as revealed by labeling for one MalPEG, due to incomplete production of DsrC-trisulfide by DsrAB (Fig. 3*C*). After the enzymatic reaction (T_f), most DsrC is now in the reduced form, as revealed by the shift for one (Cys_A) and two labeled cysteines (Cys_A and Cys_B) (Fig. 3*C*). In the control experiments, without DsrMKJOP or menadiol, DsrC remains in the oxidized DsrC-trisulfide state. Using the MalPEG assay to follow the reaction in time, the decrease in the DsrC-trisulfide band and increase in the band for reduced, doubly labeled DsrC, is clearly seen (Fig. 3*D*). Increasing concentrations of menadiol for the same reaction time also increases the extent of reaction (Fig. 3*E*). As a control, reduced DsrC was tested as a substrate for

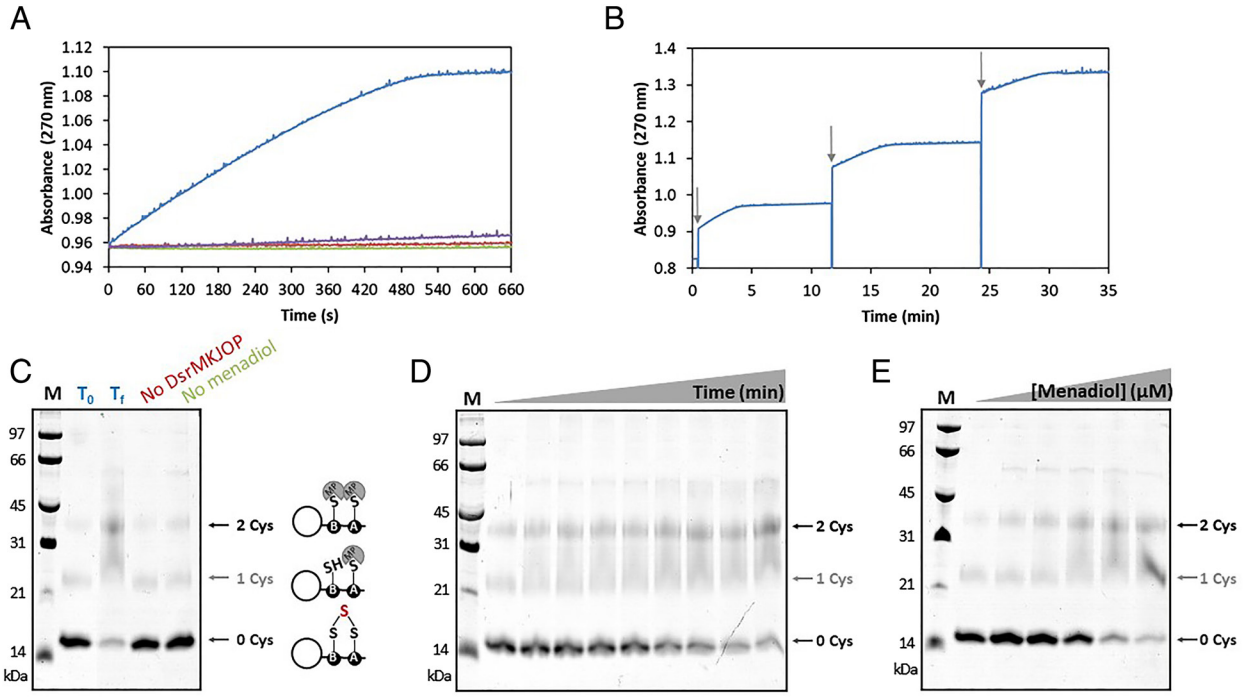

Fig. 3. Kinetic assays of the reduction of DsrC-trisulfide by the DsrMKJOP complex. (*A*) Menadiol:DsrC-trisulfide oxidoreductase activity catalyzed by *A. fulgidus* DsrMKJOP (blue), and in the absence of DsrC-trisulfide (purple), absence of DsrMKJOP (red), and absence of menadiol (green), as measured by the absorbance of the product menadione at 270 nm. (*B*) Menadiol:DsrC-trisulfide oxidoreductase activity catalyzed by *A. fulgidus* DsrMKJOP upon successive additions of DsrC-trisulfide, measured by the absorbance of the product menadione at 270 nm (arrow indicates addition of 5 μM DsrC-trisulfide). (*C* and *D*) Gel-shift analysis of MalPEG-labeled (MP) DsrC from *A (C),* and after reaction with DsrMKJOP and 0.5 mM menadiol over time (at 0, 1, 2, 3, 5, 10, 15, 20, and 30 min, *B*). MalPEG causes a shift of approximately 10 kDa per each labeled cysteine. (*E*) Gel-shift analysis of MalPEG-labeled DsrC with increasing concentrations of menadiol (0, 0.8, 4, 20, 100, and 500 μM), reacted for 30 min. (M, molecular marker; T_0, time zero; T_f, time at the end of reaction).

DsrMKJOP under the same conditions. In this case, no activity is observed (*SI Appendix*, Fig. S2*A*), as expected, and the MalPEG assay confirms the reduced state of DsrC in the beginning and end of the experiment (*SI Appendix*, Fig. S2*B*).

Finally, the redox state of DsrC C-terminal cysteines was also characterized by peptide mass fingerprinting after protein digestion with Asp-N endoproteinase, which gives rise to a small peptide containing both Cys_A and Cys_B, followed by alkylation with iodoacetamide (IA), which adds 57 Da per reduced cysteine (14). In reduced DsrC, the C-terminal peptide ^{101}DA**C**RIAGLPKPTG**C**V^{115} has a mass of 1498.7 Da (14), and upon alkylation, a peptide with 1,614.9 Da is detected (Fig. 4*A*). In the DsrC-trisulfide formed by reaction with DsrAB, the C-terminal peptide shows a mass increase of 32 Da to 1,530.7 Da, which remains unaltered by alkylation with IA (Fig. 4*B*). A small amount of unreacted IA-labeled DsrC is still detected in this sample (1,614.8 Da), as well as a species that does not react with IA (1,498.8) and likely corresponds to DsrC with a disulfide bond between the two Cys. It should be noted that the peak intensities are not directly correlated with relative amounts, as they depend on the different ionization properties of each peptide. As expected, analysis of the DsrC peptide after the reaction with DsrMKJOP, reveals the disappearance of the DsrC-trisulfide peak at 1,530.7 Da, and the increase of the 1,614.8 Da peak characteristic of reduced DsrC, where two cysteines react with IA (Fig. 4*C*).

Sulfide Is the Product of DsrMKJOP Catalysis. The products of DsrC-trisulfide reduction by the DsrMKJOP complex should be sulfide and reduced DsrC (Fig. 5*A*). To try to quantify the sulfide released during DsrMKJOP catalysis, the reaction was

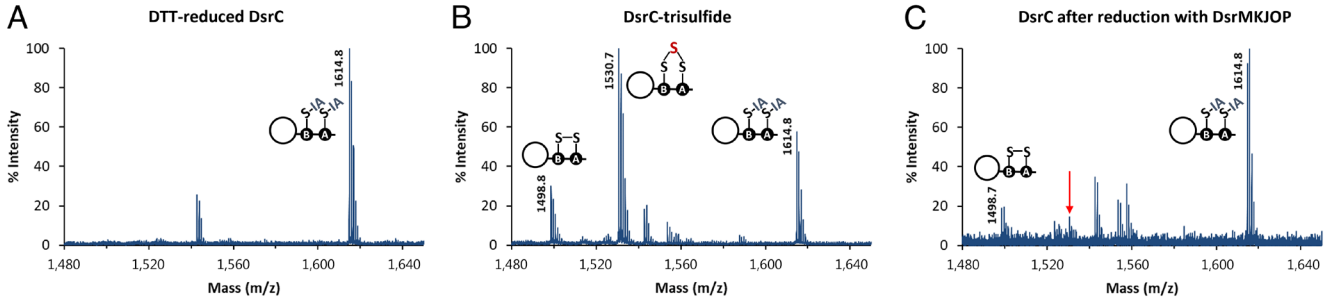

Fig. 4. Peptide mass fingerprinting spectra of DsrC C-terminal peptides after alkylation with IA. (*A*) DTT-reduced DsrC (before the reaction with *A. fulgidus* DsrAB and sulfite). (*B*) DsrC-trisulfide (produced in the in vitro enzymatic reaction with *A. fulgidus* DsrAB and sulfite). (*C*) DsrC recovered after the in vitro enzymatic reaction with *A. fulgidus* DsrMKJOP complex and menadiol. The C-terminal peptide of DsrC-trisulfide (1,530.7 Da) is marked with an arrow in (*C*) showing its disappearance relative to *B*. (IA, iodoacetamide; DTT, dithiothreitol).

performed with increasing concentrations of DsrC-trisulfide. These kinetic studies showed an increase in the length of the reaction with increasing substrate concentrations (Fig. 5*B*), but not an increase in reaction rate. This indicates that the concentrations used are already saturating and that the Michaelis–Menten constant (K_M) for the DsrC-trisulfide is probably in the nM range, in agreement with the measured K_D. The reaction rates slow down as the substrate becomes exhausted. The product sulfide, quantified by HPLC (high-performance liquid chromatography) as the monobromobimane (mBBr) fluorescent derivative, increases linearly with increasing DsrC-trisulfide concentrations (Fig. 5*C*), although in sub-stoichiometric amounts (40 to 50%). This can be explained by two factors: i) the partial escape of hydrogen sulfide to the gas phase at pH 7.0, made worse by the high temperature used for the DsrMKJOP assay (60 °C), and ii) by a degree of uncertainty associated with quantification of the DsrC-trisulfide. This quantification was performed indirectly using the BCA (bicinchoninic acid) (for protein quantification) and DTNB (5,5-dithio-bis-(2-nitrobenzoic acid)) (for thiol quantification) assays, by the amount of reduced DsrC remaining in samples of the DsrC-trisulfide. However, we observed by mass spectrometry (MS) that upon production of the DsrC-trisulfide some part of DsrC is in the disulfide state and is not alkylated by IA (peak 1,498.8 Da in Fig. 4 *B* and *C*) and thus is also not quantified by DTNB derivatization, generating an uncertainty in the actual level of DsrC-trisulfide present in the samples. Thus, the sulfide production experiment is more qualitative than quantitative. Nevertheless, the level of sulfide produced is proportional to the amount of DsrC-trisulfide in the assay, and taken globally, these results show that DsrMKJOP can catalyze full reduction of the DsrC-trisulfide to sulfide using menadiol, finally clarifying the functional role of this respiratory complex in dissimilatory sulfite reduction.

Insights into the Catalytic Mechanism of DsrMKJOP. A catalytic mechanism for heterodisulfide reduction by Hdrs has been proposed based on the structure of HdrABC with substrate bound, where the CoM-S-S-CoB heterodisulfide binds between the two noncubane $[4Fe\text{-}4S]^{3+/2+}$ clusters and is homolytically cleaved (36). The thyil radicals formed may be stabilized by coordination with the reduced $[4Fe\text{-}4S]^{2+}$ clusters, leading to the binding of the CoM and CoB sulfurs to the two $[4Fe\text{-}4S]^{3+}$ clusters, resulting in the open conformation of the clusters (37). Two consecutive single-electron reduction steps release CoB-SH and CoM-SH (36, 37). However, the catalytic mechanism of the DsrMKJOP complex is likely different since it coordinates a single noncubane $[4Fe\text{-}4S]^{3+/2+}$ cluster in DsrK instead of the two found in HdrD and HdrB (*SI Appendix*, Fig. S3). Interestingly, in many DsrK proteins from different sulfate reducers, the last cysteine of the CCG motif for binding this cluster is replaced by a conserved aspartate (*SI Appendix*, Fig. S4). In *A. fulgidus*, the DsrK protein of the DsrMKJOP complex (AF0502) has this aspartate, whereas three other DsrK homologs (AF0543 part of a *dsrMKJOP* gene set, and AF0544 and AF0547 part of *dsrMK* arrangements), have a cysteine, suggesting that both residues may be functional. In addition, one of the conserved cysteines from

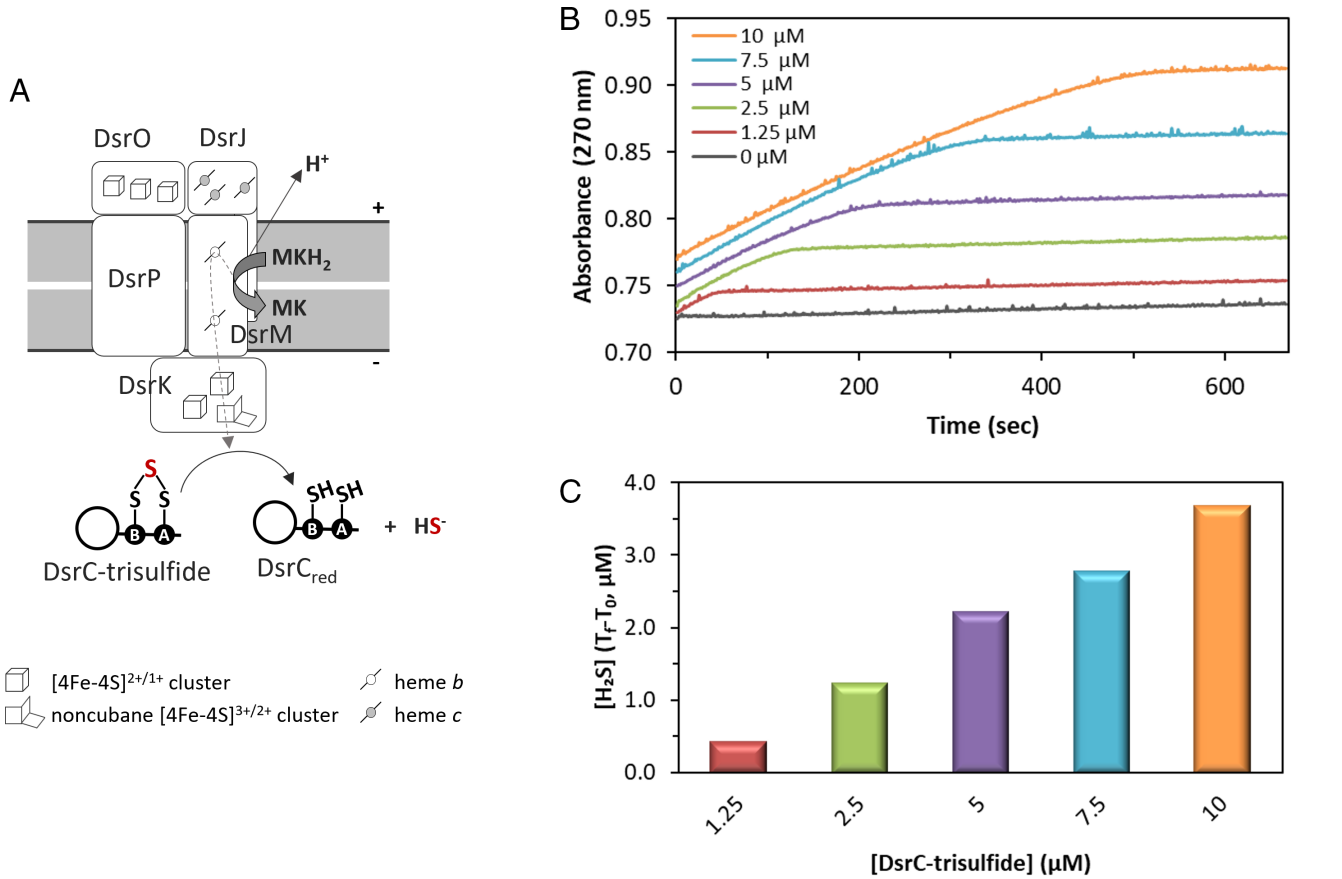

Fig. 5. Reduction of DsrC-trisulfide by DsrMKJOP and sulfide production. (*A*) Schematic representation of the reaction catalyzed by DsrMKJOP. (*B*) Menadiol:DsrC-trisulfide oxidoreductase activity catalyzed by *A. fulgidus* DsrMKJOP with increasing concentrations of DsrC-trisulfide (0 to 10 µM), measured by the absorbance of the product menadione at 270 nm. (*C*) Hydrogen sulfide produced in the reactions shown in *B*. H_2S was measured before the addition of DsrC-trisulfide (T_0) and 30 min after the start of the enzymatic reaction (T_f). The control in the absence of DsrC-trisulfide was subtracted from all points. Results from a representative experiment are shown.

the missing noncubane cluster (Cys^{329} in *A. fulgidus* numbering) is strictly conserved in DsrK proteins and is likely involved in the catalytic mechanism of DsrC-trisulfide reduction. This cysteine is part of a conserved GECGH sequence motif that is highly conserved in DsrK from several organisms (*SI Appendix*, Fig. S4) and is one of the cysteines from the second CCG signature motif in HdrD and HdrB (*SI Appendix*, Fig. S3). A similar amino-acid motif (ECGLH), present in APS and PAPS reductases, includes a redox-active catalytic cysteine (43). Other proteins from sulfate reducers, homologous to DsrK and HdrD, such as HmcF from the HmcABCDEF complex (25, 30, 44) and TmcB from the TmcABCD complex (45) also contain only one CCG motif and this conserved cysteine in a T/GECGH motif (*SI Appendix*, Fig. S3), suggesting that this cysteine is probably essential for disulfide reduction catalysis. The Hmc and Tmc complexes are both transmembrane complexes with a similar architecture to the DsrMKJOP complex, but they are not present in *A. fulgidus* (25). Interestingly, the characteristic EPR signal of the noncubane $[4Fe\text{-}4S]^{3+}$ cluster was initially reported for the methanogenic HdrB and HdrD only in the presence of HS-CoM or HS-CoB (38–40), which bind to the cluster, whereas for DsrK and TmcB proteins this signal is observed in the as-isolated protein, in the absence of any added substrate (17, 22, 45). This could suggest that this conserved cysteine might be binding the cluster and generating the open $S = ½$ conformation. However, for the recombinant HdrB protein produced in *Escherichia coli,* the signal for the noncubane cluster was visible already in the absence of substrate (29).

In methanogens, the redox potential of the CoM-S-S-CoB heterodisulfide has been determined to be $E^{0'} = -143 \pm 10$ mV vs. SHE (standard hydrogen electrode) (46), which is more positive than that of typical disulfides such as glutathione and cysteine. It is also more positive than the potential of methanophenazine ($E^{0'} = -165 \pm 6$ mV), the membrane-associated quinone-like redox carrier that is the electron donor to HdrED (46). The redox potential of the DsrC-trisulfide is unknown, so it is not clear whether its reduction by menaquinol ($E^{0'} \sim -70$ mV) is thermodynamically favorable. Protein disulfide bonds are known to span a wide range of potentials. For example, *A. fulgidus* proteins from the thioredoxin superfamily have potentials ranging from −32 to −309 mV (pH 7.0) (47). A value of −346 mV (pH 7.0, vs. SHE) has been reported for several organic water-soluble trisulfides (48), but we know of no reports for redox potentials of protein-bound trisulfides, so it is very difficult to estimate the redox potential of the DsrC-trisulfide. We tested the chemical reduction of this species by different chemical reducing agents, and surprisingly none of them, not even those with very low redox potential, could reduce the DsrC-trisulfide as analyzed with the MalPEG shift assay (*SI Appendix*, Fig. S5). Moreover, MS confirmed the intact state of the DsrC-trisulfide after reduction with dithionite, tris(2-carboxyethyl)phosphine (TCEP) and dithiothreitol (DTT) (*SI Appendix*, Table S1). This unexpected result suggests that the DsrC-trisulfide can only be reduced by the DsrMKJOP complex. The fact that it cannot be chemically reduced could suggest that it has a low redox potential, which could increase upon interaction with the DsrMKJOP complex, but it is also possible that the reduction of the trisulfide is not thermodynamically, but kinetically prevented, i.e., that the reaction has a high activation energy and occurs only when it is enzymatically catalyzed. This sort of argument has been put forward by Flohé and coworkers in discussing the glutathione redox potential and its physiological significance (49, 50). Such kinetic impediment for reduction of the DsrC-trisulfide, which may be based on steric inaccessibility of the trisulfide, makes sense considering that this species is likely to face a considerable intracellular sulfide concentration.

Nevertheless, the full reduction of the DsrC-trisulfide, as observed by MS, and the increasing production of sulfide upon reaction of DsrMKJOP and menadiol with increasing concentrations of DsrC-trisulfide confirm that its reduction by this menaquinol analog does occur. This reaction could, in principle, only involve the DsrMK subunits in analogy to HdrED, with DsrM as the menaquinol-oxidizing subunit that transfers electrons to DsrK for trisulfide reduction, and in fact, in many organisms, only these two subunits are present (2, 25). This leaves the function of the DsrJOP subunits as an enigma.

It has been suggested that the DsrJ cytochrome could react with a periplasmic sulfur substrate (17, 22, 31), due to the presence of the unusual His/Cys heme coordination that is also present in SoxXA involved in thiosulfate oxidation (51) or in TsdA thiosulfate dehydrogenase (33). We tested both thiosulfate and sulfite as electron donors to the complex and could not detect any activity with menadione and/or DsrC-trisulfide as electron acceptors, and sulfite actually decreased the rate of DsrC-trisulfide reduction by DsrMKJOP (*SI Appendix*, Fig. S6). Since the DsrJOP module is not essential for some organisms, a hypothesis is that its role is to increase the energetic efficiency of the DsrMKJOP complex vs. the DsrMK version. We have previously suggested that the DsrMK and DsrJOP modules could be involved in some form of proton-translocating quinone cycling, as present in the bc_1 complex, possibly involving quinone-based electron bifurcation (16). In addition or alternatively, the DsrJOP module may allow for proton pumping upon DsrC-trisulfide reduction. Notably, the DsrOP proteins form a quinone-interacting redox module that is widespread in bacterial oxidoreductases (11, 30), and some proteins of the DsrP family may be involved in proton pumping, such as the alternative complex III (52, 53) and the reductive dehalogenase complex (54).

In conclusion, our results are a major step forward in the molecular understanding of dissimilatory sulfur metabolism by identifying the function of the DsrMKJOP complex, showing that it interacts with the DsrC-trisulfide and acts as a menadiol:DsrC-trisulfide oxidoreductase that produces sulfide. The architecture of the DsrMKJOP complex indicates that it is quite an elaborate machine and further studies will be essential to understand its molecular mechanism and how it is coupled to energy conservation.

Materials and Methods

Purification of *A. fulgidus* DsrMKJOP. The purification protocol was adapted from a previous report (22). *A. fulgidus* VC-16 (DSM 4304) was grown in sulfate-thiosulfate-lactate medium in 300 L fermenter at 83 °C, as previously described (55), without addition of dithionite. Frozen cells were resuspended in 50 mM potassium phosphate buffer (KPi) pH 7.0, 10% (v/v) glycerol, homogenized, and disrupted in an APV Model 2000 Homogenizer at 80 MPa in the presence of DNase (Sigma-Aldrich) and cOmplete™ protease inhibitor cocktail (Roche). The cell lysate was centrifuged at 7,930 × g for 20 min at 4 °C, followed by ultracentrifugation at 138,000 × g for 2 h at 4 °C. The supernatant (soluble extract) was used to isolate *A. fulgidus* DsrAB (see below). The pellet (membrane extract) was solubilized with gentle stirring overnight at 4 °C in 50 mM potassium phosphate buffer pH 7.0, 10% (v/v) glycerol, and 2% (w/v) n-dodecyl β-D-maltoside (DDM, Glycon Biochemicals GmbH). The solubilized membrane proteins were separated by ultracentrifugation at 138,000 × *g* for 2 h at 4 °C, and the membrane pellet was used for a second solubilization for 5 h with gentle stirring at 4 °C, followed by a third ultracentrifugation step under the same conditions. The pooled solubilized membrane proteins were loaded into a Q-Sepharose high-performance column (2.6 × 10.0 cm, Amersham Pharmacia Biotech) equilibrated with buffer A (50 mM KPi pH 7.0, 10% (v/v) glycerol, 0.1% (w/v) DDM, and a cOmplete™ protease inhibitor tablet/L). A stepwise gradient of increasing concentrations of NaCl (from 0 to 1 M NaCl) was applied and the fractions eluted at 0.45 M and 0.5 M NaCl were pooled, concentrated and the ionic strength of the solution

was lowered by dilution with buffer A and ultrafiltration (50-kDa cutoff, Amicon, Millipore). The concentrate was applied to a Resource Q column (1.6 × 3.0 cm, Amersham Pharmacia Biotech) equilibrated with buffer A. A stepwise gradient of increasing concentrations of NaCl (from 0 to 1 M NaCl) was performed and the fractions eluted at 0.3 M and 0.35 M NaCl were pooled, concentrated, and the ionic strength lowered by dilution and concentration steps as above. All the chromatographic steps were performed at 4 °C, aerobically, and monitored by UV–visible spectroscopy. The purity of DsrMKJOP was analyzed by a 10% Tricine-SDS-PAGE gel and a Blue Native-PAGE gel, followed by Coomassie Blue staining and heme-staining (56), and the protein concentration was determined using the previously determined absorption coefficient (ε) of 132.4 mM^{-1} cm^{-1} at 555 nm in the reduced state (57).

UV–Visible Spectroscopy. UV–visible spectra were acquired in a Shimadzu UV-1800 spectrophotometer inside a Coy anaerobic chamber (98% N_2, 2% H_2). Spectra were obtained at 60 °C, using as-purified DsrMKJOP, prepared in 20 mM Tris-HCl (tris(hydroxymethyl)aminomethane hydrochloride) pH 7.5, then incubated with menadiol and an excess of sodium dithionite to allow full reduction. Menadiol was prepared by reduction of menadione with sodium dithionite (58), stored in a dry state at −20 °C under anoxic conditions, and solubilized in ethanol prior to use. A control spectrum of the as-purified DsrMKJOP complex was obtained by addition of the same volume of ethanol as for menadiol incubation.

EPR Spectroscopy. X-band EPR spectra were obtained on a Bruker EMX spectrometer (Billerica, MA) equipped with an Oxford Instruments ESR-900 continuous flow helium cryostat (Abingdon, UK). A menadiol-treated sample of the DsrMKJOP complex, in 20 mM Tris-HCl pH 7.5 at a concentration of 25 μM, was prepared inside a Coy anaerobic chamber (98% N_2, 2% H_2) by incubation for 2 h at 60 °C with a solution of menadiol in ethanol in a 1:500 ratio. As control, an as-purified DsrMKJOP sample was also incubated for 2 h with the same volume of ethanol as was used in the menadiol experiment. Samples were transferred to EPR tubes within the anaerobic chamber, capped, and immediately frozen in liquid nitrogen upon removal from the chamber. All spectra were recorded using a microwave frequency of 9.38 GHz, a field modulation frequency of 100 kHz, a microwave power of 20.1 mW, a modulation amplitude of 1.0 mT, and a temperature of 23 K.

Purification of *A. fulgidus* DsrAB. The purification protocol of the soluble extract from *A. fulgidus* cells followed two consecutive ion exchange chromatography steps at 4 °C under air, as described in detail in Santos et al. (14). The purity of DsrAB was analyzed in a 10% Tricine-SDS-PAGE gel, and the protein concentration was determined by UV–visible spectroscopy using an ε of 60 mM^{-1} cm^{-1} at 593 nm determined previously (14). The purified DsrAB was stored under anoxic conditions (in a gas-tight flask under N_2 atmosphere) to prevent prolonged contact with O_2, which leads to gradual activity loss.

Purification of Recombinant *A. fulgidus* DsrC. *A. fulgidus* DsrC with the two structural Cys (Cys^{77} and Cys^{85}) modified to Ala was expressed in *E. coli* and purified by an affinity exchange chromatography step on a HiTrap™ immobilized metal-ion affinity chromatography high-performance column (GE Healthcare), as described in detail in Ferreira et al. (15). The purity of DsrC was analyzed on a 10% Tricine-SDS-PAGE gel, and the protein concentration was determined by BCA assay (Merck Millipore) and by UV–visible spectroscopy using an ε of 24 mM^{-1} cm^{-1} at 280 nm. Before its use in activity assays, DsrC was treated with 5 mM dithiothreitol (DTT, Sigma-Aldrich) during 30 min at 37 °C, to ensure its Cys were in the reduced state, and excess reductant was removed with a HiTrap™ Desalting column (GE Healthcare) (14). Reduced DsrC was concentrated, if necessary, by ultrafiltration (10-kDa cutoff, Amicon Millipore) and kept under anoxic conditions (in a gas-tight flask under N_2 atmosphere) until use. The redox state of the DsrC (5 μg) was analyzed by a gel-shift assay using MalPEG (methoxy-polyethylene glycol maleimide, Fluka), as described in Venceslau et al. (42).

Production and Analysis of DsrC-Trisulfide. The enzymatic production of DsrC-trisulfide was performed inside a Coy anaerobic chamber (98% N_2, 2% H_2) at 60 °C using Zn-reduced methyl viologen (Sigma-Aldrich) as the electron donor (14). The activity assays were run in 50 mM KPi pH 7.0, 1 mM Zn-reduced methyl viologen (MV^+), 200 nM of DsrAB, 0.5 mM sodium sulfite (Sigma-Aldrich), with a range from 10 to 100 μM of reduced DsrC. After a 5-min incubation of DsrAB in the reaction buffer, followed by a 1 min incubation with DsrC, the reaction was started by addition of sodium sulfite. The oxidation of MV^+ was monitored at 732 nm (ε = 3.15 mM^{-1} cm^{-1}) in a spectrophotometer. A prolonged incubation time (from 15 to 60 min depending on the DsrC-trisulfide concentration) was used to try to drive the enzymatic reaction to completion and have DsrC as much as possible in the trisulfide form. The enzymatic solution was diluted and concentrated by ultrafiltration (10 kDa cutoff, Amicon Millipore) to remove the methyl viologen. The redox state of DsrC was monitored with the MalPEG gel-shift assay as previously described (42).

Determination of DsrC Thiol Content by DTNB. DsrC in different redox states was subject to a DTNB (DTNB–Ellman's reagent) assay to quantify the sulfhydryl groups present. DsrC (0.8 to 3 nmol) was incubated in 100 mM KPi pH 8.0, 1 mM EDTA (ethylenediamine tetraacetic acid), and 0.2 mM DTNB (Sigma-Aldrich) for 15 min at room temperature. The production of 2-nitro-5-thiobenzoate anion (TNB^{2-}) was quantified by measuring the absorbance at 412 nm using the ε of 14,150 M^{-1} cm^{-1} (59).

SPR Analysis. The SPR experiments were performed at 25 °C on a BIAcore 2000 instrument (GE Healthcare). DsrC-trisulfide was immobilized on a NTA sensor chip (GE Healthcare) by the His-tag tail present at the N terminus. All the assays were performed with 10 mM HEPES (4-(2-hydroxyethyl)piperazine-1-ethanesulfonic acid) pH 7.4, 150 mM NaCl, 50 μM EDTA, and 0.005% (v/v) Tween 20 running buffer. DsrC-trisulfide (45 nM) was bound to a previously activated flow cell at a flow rate of 5 μL/min in the presence of 500 μM $NiCl_2$ in running buffer in order to have an immobilization of around 350 resonance units (RU). Another activated flow cell was similarly treated with running buffer in the absence of DsrC-trisulfide (control cell). Interaction experiments with DsrMKJOP complex were performed with a 3 min injection of increasing concentrations of DsrMKJOP complex (range from 8.9 to 568 nM) at a flow rate of 30 μL/min. At the end of sample injection, the NTA sensor chip was regenerated with 350 mM EDTA in running buffer for 1 min at a flow rate of 10 μL/min before a new cycle of surface activation and immobilization. Sensorgrams were obtained by subtracting the unspecific binding to the control flow cell in order to remove buffer artifacts and normalizing to the baseline injection timepoint. The equilibrium dissociation constant (K_D) was determined from duplicate experiments and according to $RU_{steady\text{-}state} = (RU_{max} \times [analyte])/K_D + [analyte])$.

DsrMKJOP Activity Assays. Menadiol:DsrC-trisulfide oxidoreductase activity assays by DsrMKJOP were performed inside a Coy anaerobic chamber (98% N_2, 2% H_2) at 60 °C using menadiol as electron donor. The activity assays were run in 50 mM KPi pH 7.0, 0.5 mM menadiol, and 100 nM DsrMKJOP in the presence of DsrC-trisulfide (10 μM). The reaction was started by addition of DsrC-trisulfide after a 5-min incubation of DsrMKJOP in the reaction buffer. The oxidation of menadiol was monitored at 270 nm [using ε_{DMN} = 16 mM^{-1} cm^{-1} (60)] in a spectrophotometer. For peptide mass fingerprinting of DsrC, the enzymatic reactions were concentrated and dialyzed by ultrafiltration (10 kDa cutoff, Amicon Millipore). To monitor the redox state of DsrC cysteines, the MalPEG gel-shift assay was used (42).

Peptide Mass Fingerprinting. The redox state of DsrC cysteines was analyzed by peptide mass fingerprinting using a matrix-assisted laser desorption/ionization-time-of-flight (MALDI-TOF/TOF) mass spectrometer, as described in Santos et al. (14). Alkylation was performed inside an anaerobic chamber by incubation of DsrC with 50 mM IA (Sigma-Aldrich) in 50 mM ammonium bicarbonate pH 7.8 during 30 min at 55 °C and run on a 10% Tricine-SDS-PAGE gel (15 μg) under non-reducing conditions. The protein bands were excised, destained, and digested with Asp-N (Roche, 20 ng/μL) overnight at 37 °C. This endoproteinase generates a peptide comprising both conserved C-terminal cysteine residues, ^{101}DA**C**RIAGLPKPTG**C**V^{115}, with predicted mass of 1,500.8 Daltons (Da). The digested peptides were desalted and concentrated using POROS C18 (Empore, 3M) and eluted directly onto the MALDI plate using 1 μL of 5 mg/mL alpha-cyano-4-hydroxycinnamic acid (Sigma-Aldrich) in 50% (v/v) acetonitrile and 5% (v/v) formic acid.

The data were acquired in positive reflector MS mode using a 5800 MALDI-TOF/TOF (AB Sciex) mass spectrometer and TOF/TOF Series Explorer Software v.4.1.0 (Applied Biosystems). External calibration was performed using CalMix5 (Protea). MS data were analyzed using Data Explorer Software v.4.11 (AB Sciex) and obtained at the UniMS Unit, ITQB/iBET, Oeiras, Portugal.

Determination of Hydrogen Sulfide by HPLC. Hydrogen sulfide was quantified using mBBr derivatization (61). mBBr (Thermo Fisher Scientific) was diluted in HPLC ultrapure acetonitrile to a final concentration of 50 mM. For derivatization, 10 μL of sample from the enzymatic reaction were reacted with 3 μL of mBBr in 50 mM EPPS (4-(2-hydroxyethyl)piperazine-1-propanesulfonic acid) pH 8.0 and 5 mM

DTPA (diethylenetriaminepentaacetic acid) in a final volume of 86 µL, inside an anaerobic chamber. The reactions were incubated in the dark at room temperature for 10 min, after which 4 µL of 5 M methanesulfonic acid was added to stop the reaction. Derivatized hydrogen sulfide (sulfide dibimane) was measured by HPLC (Waters Alliance 2695) with a fluorescence detector (Waters 2475) with an excitation/emission wavelength of 380 and 480 nm, respectively, using a reverse phase Ultrasphere® ODS column (4.6 × 250 mm, 5 µm, Hichrom) run at a flow rate of 1.2 mL min^{-1} and 35 °C, as described in detail in Santos et al. (14). The retention time was 15.5 min for sulfide dibimane. A calibration curve was performed with freshly prepared solutions of sodium sulfide nonahydrate (Sigma-Aldrich) in 50 mM KPi pH 7.0, reacted with excess mBBr.

Data, Materials, and Software Availability. All study data are available from Figshare DOI: 10.6084/m9.figshare.24999161 (62).

ACKNOWLEDGMENTS. We thank João Carita and Cristina Leitão from ITQB NOVA for the growth of *A. fulgidus* and HPLC analysis, respectively. This work was funded by the Fundação para a Ciência e Tecnologia (Portugal) through Fellowships PD/BD/135488/2018 and COVID/BD/152504/2022 (A.C.C.B.), Grants PTDC/BIA-MIC/6512/2014 and PTDC/BIA-BQM/29118/2017, Research Unit Molecular, Structural and Cellular Microbiology (MOSTMICRO-ITQB) (UIDB/04612/2020 and UIDP/04612/2020), and Associate Laboratory Life Sciences for a Healthy and Sustainable Future (LS4FUTURE) (LA/P/0087/2020).

1. G. Muyzer, A. J. M. Stams, The ecology and biotechnology of sulphate-reducing bacteria. *Nat. Rev. Microbiol.* **6**, 441–454 (2008).
2. R. Rabus *et al.*, A post-genomic view of the ecophysiology, catabolism and biotechnological relevance of sulphate-reducing prokaryotes. *Adv. Microb. Physiol.* **66**, 55–321 (2015).
3. B. B. Jørgensen, A. J. Findlay, A. Pellerin, The biogeochemical sulfur cycle of marine sediments. *Front. Microbiol.* **10**, 1–27 (2019).
4. S. E. McGlynn, G. L. Chadwick, C. P. Kempes, V. J. Orphan, Single cell activity reveals direct electron transfer in methanotrophic consortia. *Nature* **526**, 531–535 (2015).
5. G. Wegener, V. Krukenberg, D. Riedel, H. E. Tegetmeyer, A. Boetius, Intercellular wiring enables electron transfer between methanotrophic archaea and bacteria. *Nature* **526**, 587–590 (2015).
6. M. Diao *et al.*, Global diversity and inferred ecophysiology of microorganisms with the potential for dissimilatory sulfate/sulfite reduction. *FEMS Microbiol. Rev.* **47**, fuad058 (2023).
7. B. T. Hanson *et al.*, Sulfoquinovose is a select nutrient of prominent bacteria and a source of hydrogen sulfide in the human gut. *ISME J.* **15**, 2779–2791 (2021).
8. S. Devkota, E. B. Chang, Interactions between diet, bile acid metabolism, gut microbiota, and inflammatory bowel diseases. *Dig. Dis.* **33**, 351–356 (2015).
9. P. G. Wolf *et al.*, Diversity and distribution of sulfur metabolic genes in the human gut microbiome and their association with colorectal cancer. *Microbiome* **10**, 1–16 (2022).
10. D. E. Canfield, M. T. Rosing, C. Bjerrum, Early anaerobic metabolisms. *Philos. Trans. R Soc. B Biol. Sci.* **361**, 1819–1836 (2006).
11. A. G. Duarte *et al.*, An electrogenic redox loop in sulfate reduction reveals a likely widespread mechanism of energy conservation. *Nat. Commun.* **9**, 5448 (2018).
12. T. F. Oliveira *et al.*, The crystal structure of *Desulfovibrio vulgaris* dissimilatory sulfite reductase bound to DsrC provides novel insights into the mechanism of sulfate respiration. *J. Biol. Chem.* **283**, 34141–34149 (2008).
13. A. R. Ramos, K. L. Keller, J. D. Wall, I. A. Cardoso Pereira, The membrane QmoABC complex interacts directly with the dissimilatory adenosine 5′-phosphosulfate reductase in sulfate reducing bacteria. *Front. Microbiol.* **3**, 137 (2012).
14. A. A. Santos *et al.*, A protein trisulfide couples dissimilatory sulfate reduction to energy conservation. *Science* **350**, 1541–1545 (2015).
15. D. Ferreira *et al.*, The DsrD functional marker protein is an allosteric activator of the DsrAB dissimilatory sulfite reductase. *Proc. Natl. Acad. Sci. U.S.A.* **119**, e2118880119 (2022).
16. S. S. Venceslau, Y. Stockdreher, C. Dahl, I. A. C. Pereira, The "bacterial heterodisulfide" DsrC is a key protein in dissimilatory sulfur metabolism. *Biochim. Biophys. Acta Bioenerg.* **1837**, 1148–1164 (2014).
17. R. H. Pires *et al.*, Characterization of the *Desulfovibrio desulfuricans* ATCC 27774 DsrMKJOP complex–A membrane-bound redox complex involved in the sulfate respiratory pathway. *Biochemistry* **45**, 249–262 (2006).
18. A. S. Pott, C. Dahl, Sirohaem sulfite reductase and other proteins encoded by genes at the *dsr* locus of *Chromatium vinosum* are involved in the oxidation of intracellular sulfur. *Microbiology (N.Y.)* **144**, 1881–1894 (1998).
19. C. Dahl, "A biochemical view on the biological sulfur cycle" in *Environmental Technologies to Treat Sulphur Pollution: Principles and Engineering*, P. N. L. Lens, Ed. (IWA Publishing, 2020), pp. 55–96.
20. J. Simon, P. M. H. Kroneck, Microbial sulfite respiration. *Adv. Microb. Physiol.* **62**, 45–117 (2013).
21. K. Wasmund, M. Mußmann, A. Loy, The life sulfuric: Microbial ecology of sulfur cycling in marine sediments. *Environ. Microbiol. Rep.* **9**, 323–344 (2017).
22. G. J. Mander, E. C. Duin, D. Linder, K. O. Stetter, R. Hedderich, Purification and characterization of a membrane-bound enzyme complex from the sulfate-reducing archaeon *Archaeoglobus fulgidus* related to heterodisulfide reductase from methanogenic archaea. *Eur. J. Biochem.* **269**, 1895–1904 (2002).
23. F. Grein, I. A. C. Pereira, C. Dahl, Biochemical characterization of individual components of the *Allochromatium vinosum* DsrMKJOP transmembrane complex aids understanding of complex function in vivo. *J. Bacteriol.* **192**, 6369–6377 (2010).
24. J. Sander, S. Engels-Schwarzlose, C. Dahl, Importance of the DsrMKJOP complex for sulfur oxidation in *Allochromatium vinosum* and phylogenetic analysis of related complexes in other prokaryotes. *Arch. Microbiol.* **186**, 357–366 (2006).
25. I. A. C. Pereira *et al.*, A comparative genomic analysis of energy metabolism in sulfate reducing bacteria and archaea. *Front. Microbiol.* **2**, 25–36 (2011).
26. S. Heiden, R. Hedderich, E. Setzke, R. K. Thauer, Purification of a two-subunit cytochrome-*b*-containing heterodisulfide reductase from methanol-grown *Methanosarcina barkeri*. *Eur. J. Biochem.* **221**, 855–861 (1994).
27. A. Künkel, M. Vaupel, S. Heim, R. K. Thauer, R. Hedderich, Heterodisulfide reductase from methanol-grown cells of *Methanosarcina barkeri* is not a flavoenzyme. *Eur. J. Biochem.* **244**, 226–234 (1997).
28. R. Hedderich, N. Hamann, M. Bennati, Heterodisulfide reductase from methanogenic archaea: A new catalytic role for iron-sulfur cluster. *Biol. Chem.* **386**, 961–970 (2005).
29. N. Hamann *et al.*, A cysteine-rich CCG domain contains a novel [4Fe-4S] cluster binding motif as deduced from studies with subunit B of heterodisulfide reductase from *Methanothermobacter marburgensis*. *Biochemistry* **46**, 12875–12885 (2007).
30. A. G. Duarte *et al.*, Redox loops in anaerobic respiration–The role of the widespread NrfD protein family and associated dimeric redox module. *Biochim. Biophys. Acta Bioenerg.* **1862**, 148416 (2021).
31. F. Grein *et al.*, DsrJ, an essential part of the DsrMKJOP transmembrane complex in the purple sulfur bacterium allochromatium vinosum, is an unusual triheme cytochrome *c*. *Biochemistry* **49**, 8290–8299 (2010).
32. M. R. Cheesman, P. J. Little, B. C. Berks, Novel heme ligation in a *c*-type cytochrome involved in thiosulfate oxidation: EPR and MCD of SoxAX from *Rhodovulum sulfidophilum*. *Biochemistry* **40**, 10562–10569 (2001).
33. K. Denkmann *et al.*, Thiosulfate dehydrogenase: A widespread unusual acidophilic *c*-type cytochrome. *Environ. Microbiol.* **14**, 2673–2688 (2012).
34. J. Alric *et al.*, Structural and functional characterization of the unusual triheme cytochrome bound to the reaction center of *Rhodovulum sulfidophilum*. *J. Biol. Chem.* **279**, 26090–26097 (2004).
35. F. Grein, A. R. Ramos, S. S. Venceslau, I. A. C. Pereira, Unifying concepts in anaerobic respiration: Insights from dissimilatory sulfur metabolism. *Biochim. Biophys. Acta Bioenerg.* **1827**, 145–160 (2013).
36. T. Wagner, J. Koch, U. Ermler, S. Shima, Methanogenic heterodisulfide reductase (HdrABC-MvhAGD) uses two noncubane [4Fe-4S] clusters for reduction. *Science* **357**, 699–703 (2017).
37. V. Pelmenschikov *et al.*, Substrate-dependent conformational switch of the noncubane [4Fe-4S] cluster in heterodisulfide reductase HdrB. *J. Am. Chem. Soc.* **145**, 7–11 (2023).
38. S. Madadi-Kahkesh *et al.*, A paramagnetic species with unique EPR characteristics in the active site of heterodisulfide reductase from methanogenic archaea. *Eur. J. Biochem.* **268**, 2566–2577 (2001).
39. E. C. Duin, C. Bauer, B. Jaun, R. Hedderich, Coenzyme M binds to a [4Fe-4S] cluster in the active site of heterodisulfide reductase as deduced from EPR studies with the [^{33}S]coenzyme M-treated enzyme. *FEBS Lett.* **538**, 81–84 (2003).
40. E. C. Duin, S. Madadi-Kahkesh, R. Hedderich, M. D. Clay, M. K. Johnson, Heterodisulfide reductase from *Methanothermobacter marburgensis* contains an active-site [4Fe-4S] cluster that is directly involved in mediating heterodisulfide reduction. *FEBS Lett.* **512**, 263–268 (2002).
41. B. Douzi, "Protein-protein interactions: Surface plasmon resonance" in *Bacterial Protein Secretion Systems*. L. Journet, E. Cascales (Eds.) (*Methods in Molecular Biology*, Humana, New York, NY, 2017), pp. 257–275.
42. S. S. Venceslau *et al.*, Redox states of *Desulfovibrio vulgaris* DsrC, a key protein in dissimilatory sulfite reduction. *Biochem. Biophys. Res. Commun.* **441**, 732–736 (2013).
43. D. P. Bhave, J. A. Hong, R. L. Keller, C. Krebs, K. S. Carroll, Iron-sulfur cluster engineering provides insight into the evolution of substrate specificity among sulfonucleotide reductases. *ACS Chem. Biol.* **7**, 306–315 (2012).
44. M. Rossi *et al.*, The *hmc* operon of *Desulfovibrio vulgaris* subsp. *vulgaris* Hildenborough encodes a potential transmembrane redox protein complex. *J. Bacteriol.* **175**, 4699–4711 (1993).
45. P. M. Pereira, M. Teixeira, A. V. Xavier, R. O. Louro, I. A. C. Pereira, The Tmc complex from *Desulfovibrio vulgaris* Hildenborough is involved in transmembrane electron transfer from periplasmic hydrogen oxidation. *Biochemistry* **45**, 10359–10367 (2006).
46. M. Tietze *et al.*, Redox potentials of methanophenazine and CoB–S–S–CoM, factors involved in electron transport in methanogenic archaea. *ChemBioChem* **4**, 333–335 (2003).
47. S. E. Chobot, H. H. Hernandez, C. L. Drennan, S. J. Elliott, Direct electrochemical characterization of archaeal thioredoxins. *Angew. Chem. Int. Ed.* **46**, 4145–4147 (2007).
48. A. Zöphel, M. C. Kennedy, H. Beinert, P. M. H. Kroneck, Investigations on microbial sulfur respiration. *Arch. Microbiol.* **150**, 72–77 (1988).
49. L. Flohé, The fairytale of the GSSG/GSH redox potential. *Biochim. Biophys. Acta* **1830**, 3139–3142 (2013).
50. C. Berndt, C. H. Lillig, L. Flohé, Redox regulation by glutathione needs enzymes. *Front. Pharmacol.* **5**, 168 (2014).
51. V. A. Bamford *et al.*, Structural basis for the oxidation of thiosulfate by a sulfur cycle enzyme. *EMBO J.* **21**, 5599–5610 (2002).
52. J. S. Sousa *et al.*, Structural basis for energy transduction by respiratory alternative complex III. *Nat. Commun.* **9**, 1728 (2018).
53. C. Sun *et al.*, Structure of the alternative complex III in a supercomplex with cytochrome oxidase. *Nature* **557**, 123–126 (2018).
54. A. Kublik *et al.*, Identification of a multi-protein reductive dehalogenase complex in *Dehalococcoides mccartyi* strain CBDB1 suggests a protein-dependent respiratory electron transport chain obviating quinone involvement. *Environ. Microbiol.* **18**, 3044–3056 (2016).
55. K. O. Stetter, G. Lauerer, M. Thomm, A. Neuner, Isolation of extremely thermophilic sulfate reducers: Evidence for a novel branch of archaebacteria. *Science* **236**, 822–824 (1987).
56. R. T. Francis, R. R. Becker, Specific indication of hemoproteins in polyacrylamide gels using a double-staining process. *Anal. Biochem.* **136**, 509–514 (1984).
57. S. S. Venceslau, "Electron transfer chains in sulfate reducing bacteria", Ph. D. Thesis Dissertation, Instituto de Tecnologia e Química Biológica António Xavier, Universidade Nova de Lisboa, Oeiras, Portugal (2011).
58. L. F. Fieser, Convenient procedures for the preparation of antihemorrhagic compounds. *J. Biol. Chem.* **133**, 391–396 (1940).
59. P. W. Riddles, R. L. Blakeley, B. Zerner, Reassessment of Ellman's reagent. *Methods Enzymol.* **91**, 49–60 (1983).
60. J. H. Weiner *et al.*, A mutant of *Escherichia coli* fumarate reductase decoupled from electron transport. *Proc. Natl. Acad. Sci. U.S.A.* **83**, 2056–2060 (1986).
61. R. C. Fahey, G. L. Newton, Determination of low-molecular-weight thiols using monobromobimane fluorescent labeling and high-performance liquid chromatography. *Methods Enzymol.* **143**, 85–96 (1987).
62. I. A. C. Pereira, S. S. Venceslau, A. C. C. Barbosa, Data_PaperDsrMKJOP_PNAS_2024.xlsx. figshare. https://doi.org/10.6084/m9.figshare.24999161.v1. Deposited 15 January 2024.